ACCSCIENCE PUBLISHING

International Journal of Bioprinting

RESEARCH ARTICLE

Fabrication of biomimetic corneas featuring epithelial, stromal, and endothelial layers via bioprinting

Tong Zhu[1,2†], Renhao Ni[1†], Haowen Sun[1,3], Shengkai Yu[1], Xu Cao[1,4], Shang Chen[1], Jingyu Shi[4], Cuicui Su[1], Yang Luo[1,4*], Lu Yang[2*], and Hua Zhang[1*]

[1]Research Institute of Smart Medicine and Biological Engineering, Health Science Center, Ningbo University, Ningbo, Zhejiang, China

[2]Department of Ophthalmology, The First Affiliated Hospital of Ningbo University, Ningbo, Zhejiang, China

[3]College of Pharmacy, Guizhou University of Traditional Chinese Medicine, Guiyang, Guizhou, China

[4]Department of Urology, The First Affiliated Hospital of Ningbo University, Ningbo, Zhejiang, China

[†]These authors contributed equally to this work.

***Corresponding authors:**
Yang Luo
(2101140092@nbu.edu.cn)

Lu Yang
(yanglu@nbu.edu.cn)

Hua Zhang
(zhanghua@nbu.edu.cn)

Citation: Zhu T, Ni R, Sun H, *et al.* Fabrication of biomimetic corneas featuring epithelial, stromal, and endothelial layers via bioprinting. *Int J Bioprint*. 2026;12(1):448-466. doi: 10.36922/IJB025380380

Received: September 15, 2025
1st revised: November 1, 2025
2nd revised date: November 28, 2025
3rd revised date: December 10, 2025
Accepted: December 12, 2025
Published online: December 18, 2025

Abstract

The bioengineering of full-thickness corneal substitutes presents significant challenges, primarily due to the complex stratified structure of the cornea, which consists of the epithelium, stroma, and endothelium, as well as its critical functional requirements, including optical transparency, mechanical stability, and biocompatibility. Herein, we present an integrated fabrication strategy that combines embedded hydrogel bioprinting with subsequent two-dimensional endothelial cell seeding to create biomimetic corneal structures using a gelatin methacryloyl (GelMA)/hyaluronic acid methacryloyl (HAMA) composite hydrogel. The engineered scaffold successfully recapitulates the native cornea's trilaminar architecture (epithelium, stroma, and endothelium) and exhibits 30–80% optical transparency across the visible spectrum. The hybrid hydrogel exhibits optimal wettability (a contact angle of approximately 50° and minimal swelling of less than 10%) and controlled degradation kinetics, effectively addressing the limitations of single-component hydrogels. The scaffold maintains structural integrity during suturing and supports robust cellular proliferation and migration. Gene expression analysis revealed the phenotypic orientation of seeded cells toward key corneal lineages, with upregulation of epithelial (*Klf4* and *Pax6*), stromal (*Col1a1* and *Col4a4*), and endothelial (*Zeb1* and *Foxc1*) markers. Overall, the bioprinted GelMA/HAMA biomimetic cornea presents a promising proof of concept for a trilayered tissue-engineered corneal construct.

Keywords: Biomimetic cornea; Hydrogel; Multi-cell types; Three-dimensional bioprinting; Tissue engineering

1. Introduction

The cornea is the transparent tissue at the front of the eye, primarily responsible for refracting light and protecting the internal structures of the eye.[1] It is vulnerable to infections caused by bacteria, viruses, and fungi, as well as to physical injuries and chemical damage, leading to corneal blindness in approximately 10 million people worldwide.[2] Although allogeneic corneal transplantation remains the gold-standard therapeutic intervention, its widespread application is constrained by severe donor shortages and inherent risks of immune rejection.[3] Moreover, despite donor screening, allografts carry additional risks of transmissible infections (e.g., hepatitis and human immunodeficiency viruses), prion diseases, and microbial keratitis.[4] Beyond the risks associated with allografts, conditions such as dystrophies, keratoconus, and other noninfectious opacities further underscore the need for safer, standardized bioengineered substitutes.[5] Thus, there is a pressing clinical need to develop bioengineered corneal substitutes.[6]

Anatomically, the cornea comprises five principal layers: the epithelium, Bowman's layer, stroma, Descemet's membrane, and endothelium. Each layer has distinct barrier, biomechanical, and optical functions, which impose stringent design requirements on engineered substitutes. Current tissue-engineering approaches have yielded various corneal substitutes utilizing natural polymers, synthetic materials, or their hybrid composites.[7] Although these constructs successfully replicate corneal components and biochemical cues, limitations such as the difficulty in reconstructing the stratified corneal structure (epithelium–stroma–endothelium), the lack of precise spatial organization of multiple cell types, inadequate mechanical stability for suturing, and low optical transparency restrict their application.[8] Among these challenges, the development of multilayered biomimetic constructs with precise spatial cell distributions remains the most formidable obstacle, due to the native cornea's complex asphericity and gradient thickness (ranging from 500 to 700 μm).[9]

Hydrogels are playing an increasingly transformative role in advancing ocular tissue engineering. For instance, Vijayaraghavan et al.[10] created three-dimensional (3D)-bioprinted corneal mimics using gelatin methacryloyl (GelMA)-methylcellulose blends that support keratocyte phenotype and display favorable transparency. Cai et al.[11] reported an injectable, self-healing zwitterionic hydrogel with stable intraocular performance in vitrectomy models. Kim et al.[12] further engineered a retina-on-a-chip with functional blood–retina barriers using multinozzle bioprinting of decellularized extracellular matrix bioinks, enabling pathological modeling of retinal vein occlusion. These studies collectively highlight the potential of advanced hydrogels and bioprinting to address the global shortage of donor corneas.[7] Among various bioprinting technologies, digital light processing (DLP) excels at fabricating corneal stromal layers with precise microarchitecture due to its high resolution (10–50 μm) and rapid fabrication speed.[13] Utilizing photopolymerization principles, this noncontact approach achieves exceptional control over corneal curvature gradients and surface topography.[14] However, the application of DLP in cell-laden, full-thickness constructs is constrained by light-path attenuation and scattering caused by cellular components and photoinitiators. This phenomenon necessitates higher light doses, which can induce phototoxicity and compromise transparency.[15] In contrast, microextrusion bioprinting excels at constructing complex, multilayered corneal architectures by enabling synchronous deposition of multiple bioinks and cell types.[16] This capability facilitates the 3D heterotypic organization of epithelium–stroma–endothelium structures, which is essential for functional corneal regeneration.[17] Nevertheless, this approach presents a resolution–viability trade-off, as maintaining > 85% viability typically requires filament diameters of 100–250 μm.[18] This limitation hinders the fabrication of ultrathin, curved constructs featuring cellular layers as narrow as 3–5 cells, while preserving structural and functional integrity.[14]

The microextrusion printability of cell-laden hydrogels, particularly in terms of cell viability and the structural integrity of the printed constructs, is closely related to the flow properties of the hydrogel inks, the sol–gel transition, and the stiffness of the gels.[19] Shear thinning of the hydrogel inks enhances extrusion fluidity and reduces shear stress that can harm cells.[20] Rapid gelation is crucial and must occur within seconds after extrusion, with the hydrogel's elastic modulus postgelation required to exceed 50 kPa to ensure shape fidelity and effectively support the printed structure.[21] For instance, Puistola et al.[22] developed a hyaluronic acid hydrogel ink exhibiting shear-thinning characteristics and an elastic modulus of 112.2 kPa via the dynamic crosslinking of aldehyde-functionalized hyaluronic acid and dopamine-carbodihydrazide-modified hyaluronic acid. Utilizing microextrusion printing technology, they successfully fabricated a bilayer hydrogel corneal structure with a 12 mm diameter, comprising a 320 μm-thick stromal layer and a 240 μm-thick epithelial layer. Similarly, Xu et al.[14] constructed a convex corneal implant using 3D printing of GelMA and collagen type I as composite inks. By regulating the temperature of the printing ink and optimizing photocuring conditions, a biomimetic cornea with a curved architecture and thicknesses ranging from 186 to 625 μm was produced. To provide adequate

structural support for the thin, curved construct, the hydrogel's compressive modulus was increased to 130 kPa, rendering the scaffold effective for surface cell seeding but incompatible with 3D cell-laden printing.[23] Despite these advancements in structural biomimicry, achieving a multilayered and multicellular construct that accurately replicates the functional equivalence of native corneas remains a considerable challenge. These difficulties primarily arise from the complexities involved in achieving the printability of multicellular biomimetic hydrogels.

To address the challenge of printing thin, curved corneas using microextrusion printing hydrogel, we developed an integrated "3D-3D-two-dimensional (2D)" fabrication strategy that combines embedded bioprinting of a stromal/epithelial cell-laden hydrogel with subsequent

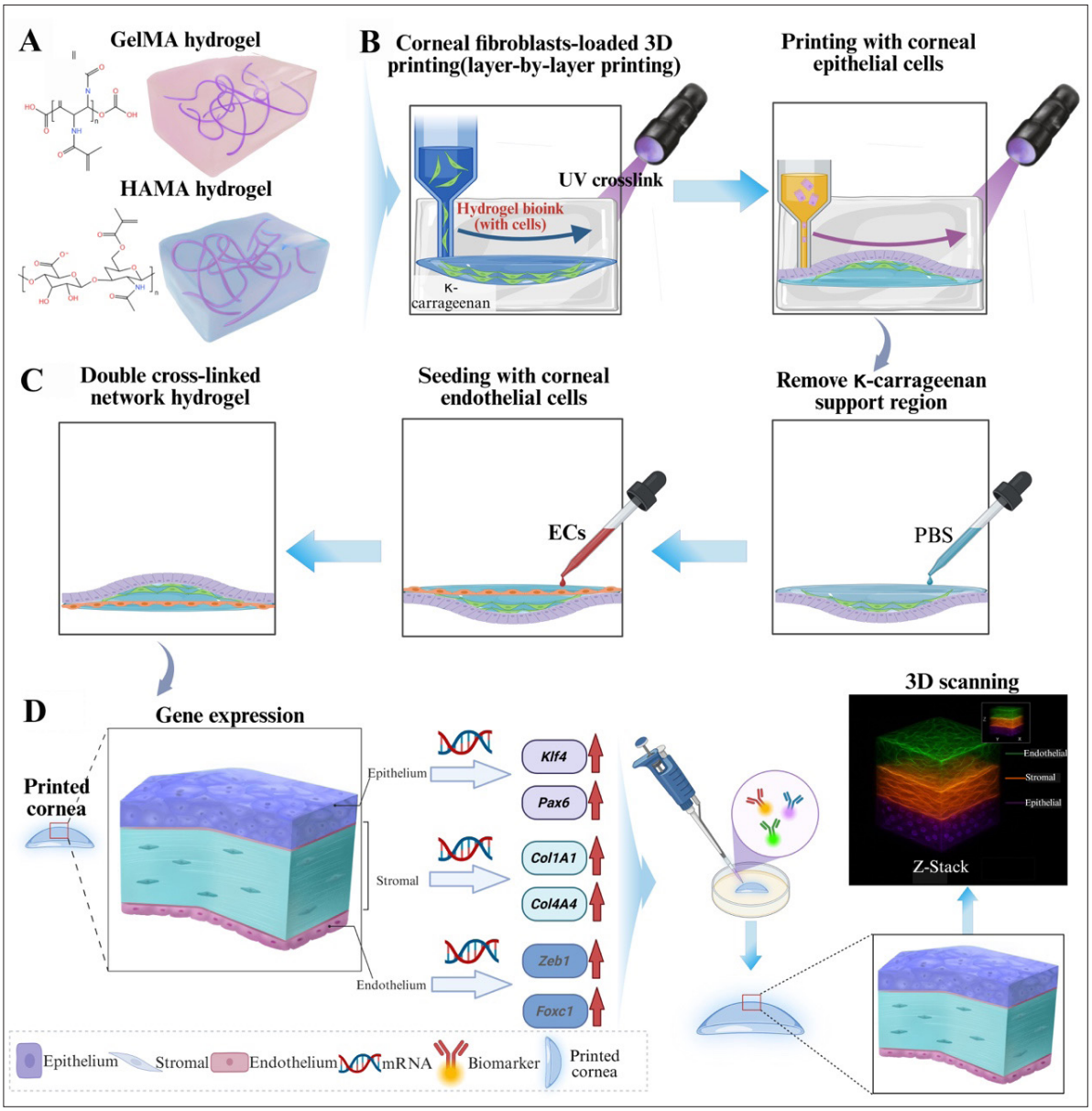

Figure 1. Schematic illustration of the construction and analysis of a trilayered 3D bioengineered cornea. (A) Molecular structures of GelMA/HAMA hydrogel bioinks. (B,C) Embedded 3D printing of the stromal (B) and epithelial (C) layers in a κ-carrageenan support bath. (D) Removal of the κ-carrageenan support bath. (E) Seeding of endothelial cells to form the trilayered construct. (F) Depiction of the resulting trilayer construct within a dual-crosslinked network. (G,H) Characterization by layer-specific quantitative polymerase chain reaction (G) and 3D confocal imaging (H) of architecture and interfaces. Abbreviations: 3D: Three-dimensional; Ecs: Endothelial cells; GelMA: Gelatin methacryloyl; HAMA: Hyaluronic acid methacryloyl; PBS: Phosphate-buffered saline; UV: Ultraviolet.

endothelial cell seeding to create a trilayered, biomimetic corneal equivalent (Figure 1). We designed a thermally and photocrosslinkable composite hydrogel of GelMA and hyaluronic acid methacrylate (HAMA) to encapsulate corneal epithelial and stromal cells (Figure 1A). The GelMA/HAMA composite exhibited temperature-sensitive physical gelation, allowing for immediate shape retention during embedded printing, followed by photopolymerization to form a stable covalent network that maintained the delicate curved structure (Figure 1B). The incorporation of HAMA into the GelMA network was optimized to achieve greater transparency and wettability compared to GelMA alone. Comprehensive rheological characterization confirmed optimal shear-thinning behavior and tunable sol–gel transitions responsive to both thermal and photochemical stimuli, facilitating the effective printing of biomimetic corneal hydrogel scaffolds. Cellular assays, including 2D surface seeding and coculturing, confirmed the biocompatibility and migratory capabilities of the GelMA/HAMA biomimetic corneal hydrogel. We successfully engineered a biomimetic corneal structure with distributed epithelial, stromal, and endothelial cells (Figure 1C). This construct significantly facilitated the 3D survival and growth of epithelial and stromal cells, alongside elevated expression of relevant genes (Figure 1D). This study lays the foundation for the future engineering of functional corneal tissue.

2. Materials and methods

2.1. Synthesis of gelatin methacryloyl

Porcine skin gelatin (100 g; Sigma-Aldrich, USA) was dissolved in phosphate-buffered saline (PBS, 1 L, pH 7.4; VivaCell, China) at 50°C with constant stirring. Methacrylic anhydride (MA, 20 mL; Sigma-Aldrich, USA) was added dropwise, and the reaction was maintained at 50°C for 3 h. The reaction mixture was then transferred to dialysis tubing (molecular weight cutoff [MWCO] 8–10 kDa) and dialyzed against deionized water at 37°C for 4 days, with the water being changed twice daily. Finally, the retentate was lyophilized to obtain GelMA as a white porous foam.

2.2. Synthesis of hyaluronic acid methacryloyl

Sodium hyaluronate (3 g) was dissolved in ice-cold deionized water (300 mL) with stirring at 4°C. After complete dissolution, MA (5.5 mL) was added slowly, and the pH of the reaction mixture was maintained at approximately 8.0 by dropwise addition of 10 mol L^{-1} sodium bicarbonate. The resulting mixture was then transferred to dialysis tubing (MWCO 8–10 kDa) and dialyzed against deionized water for 7 days, with the water being changed daily. Finally, the retentate was freeze-dried to yield HAMA.

2.3. Nuclear magnetic resonance spectroscopy analysis

Samples of gelatin, GelMA, hyaluronic acid, and HAMA (≈50 mg each) were dissolved in 600 µL deuterium oxide. ^{1}H nuclear magnetic resonance (NMR) spectra were recorded at 400 MHz using an NMR spectrometer (AVANCE III 400 Bruker, Germany) at 25°C. For GelMA, the methacrylate vinyl protons were integrated over the range of 5.3–6.1 ppm (I_{vinyl}) and normalized to the gelatin α-CH region at 3.9–4.5 ppm ($I_{\alpha\text{-CH}}$). The degree of methacrylation (DoM) was calculated using **Equation (1).**

$$DoM\,(\%) = \frac{\frac{I_{vinyl}}{3}}{\frac{I_{\alpha-CH}}{1}} \times 100\% \quad (1)$$

For HAMA, I_{vinyl} (5.3–6.1 ppm) was normalized to the invariant N-acetyl–CH_3 signal at 1.90 ppm ($I_{Ac\text{-}CH3}$), resulting in **Equation (2).**

$$DoM\,(\%) = \frac{\frac{I_{vinyl}}{3}}{\frac{I_{Ac-CH3}}{3}} \times 100\% = \frac{I_{vinyl}}{I_{Ac-CH3}} \times 100\% \quad (2)$$

All integrations were performed using MestReNova software (Version 14.0, Mestrelab Research S.L., Spain) with automatic phase and baseline correction. For each material, ^{1}H NMR spectra were recorded from independently synthesized batches (n = 3). The DoM was calculated for each batch as described above, and the results are reported as mean ± standard deviation (SD).

2.4. Preparation of gelatin methacryloyl/hyaluronic acid methacryloyl mixed solution and hydrogel

Separate stock solutions of GelMA (10 g) and HAMA (1 g) were prepared in PBS at concentrations of 20% (w/v) and 2% (w/v), respectively. These stock solutions were then mixed at a 1:1 volume ratio, and lithium phenyl-2,4,6-trimethylbenzoylphosphinate (LAP, 0.03 g) was added to a final concentration of 0.3% (w/v), yielding the final precursor solution (10% GelMA + 1% HAMA). Control precursors of 10% GelMA and 1% HAMA were prepared identically. All solutions were photopolymerized under 405 nm near-ultraviolet (UV) light (10 mW cm^{-2}) for 60 s.

2.5. Contact angle and hydrophilicity

Hydrogel disks (≈2 mm thick) were prepared in silicone molds via UV-curing. Static water contact angles were measured at 25°C and 50–60% relative humidity using a goniometer (DSA100, Kruss, Germany). A 2 μL droplet of ultrapure water was deposited on the hydrogel surface, and the contact angle was measured within 5 s of droplet settlement. For each hydrogel disk (sample), three random locations were measured, and the values were averaged to represent the sample's contact angle. For each hydrogel formulation, three independently prepared disks (n = 3) were analyzed. Data are reported as mean ± SD.

2.6. Transmittance

The optical transparency of each hydrogel formulation was quantified using a UV–visible (UV–vis) spectrophotometer (UV-2600, Shimadzu, Japan). Square films (~1 mm thick) were equilibrated in PBS for 24 h, blotted to remove surface moisture, and mounted in quartz cuvettes. Transmittance spectra were collected from 380 to 780 nm at a scan rate of 1 nm s^{-1}, using deionized water as the baseline. For each formulation, three independently prepared hydrogels were measured (n = 3), and the spectra are reported as mean ± SD. The transmittance (T, %) was calculated using **Equation (3)**

$$T(\%) = \frac{I}{I_0} \times 100\% \quad (3)$$

where I is the transmitted light intensity of the sample, and I_0 is the background transmitted light intensity.

2.7. Rheological properties of hydrogels and *κ*-carrageenan

The rheological properties were characterized using a rheometer (Discovery HR-20, TA Instruments, USA) equipped with a 60 mm diameter parallel plate geometry and a Peltier temperature control system. All measurements were performed with a fixed gap of 500 μm. A temperature sweep was conducted from 20 to 40°C at a heating rate of 5°C min^{-1} to characterize the thermoresponsive behavior. Steady-state flow measurements were performed by recording the viscosity over a shear rate range of 0.001–1,000 s^{-1} after equilibrating the sample at 37°C for 5 min. To monitor photocrosslinking kinetics, time-sweep measurements were initiated, and the sample was immediately exposed to continuous 405 nm irradiation at 10 mW cm^{-2}. The flow curves of κ-carrageenan precursor solutions (0.2–0.5% w/v) were obtained in shear ramp mode by applying a logarithmic shear rate ramp from 0.01 to 1,000 s^{-1} at 37°C. The κ-carrageenan solutions were subjected to a test that alternated between a high-shear destruction phase (100 s^{-1} for 60 s) and a low-shear recovery phase (0.01 s^{-1} for 60 s) to quantify the time-dependent recovery of viscosity.

2.8. 3D bioprinting of biomimetic corneal constructs

A biomimetic corneal template was designed in Rhino (Version 7, Robert McNeel & Associates, USA) and processed in Pango (Version 2.1.1, Panowin, China) with the following parameters: 160 μm layer height, filament width matching the nozzle inner diameter, 100% concentric infill to mimic the lamellar architecture, 60 mm s^{-1} printing speed, and 80 mm s^{-1} travel speed, all optimized to maximize geometric fidelity. The bioink was prepared by dissolving 10% GelMA and 1% HAMA in sterile PBS (pH 7.4) containing 0.30% (w/v) LAP as a photoinitiator. The mixture was gently blended at 37°C and degassed by centrifugation (2,000 rpm, 5 min), then maintained at 37°C until printing. A granular 0.4% κ-carrageenan support bath (8–10 mm depth) was pre-equilibrated to 15°C to facilitate rapid physical gelation upon ink deposition. The prepared bioink was loaded into a 5 mL syringe equipped with a 160 μm inner-diameter steel nozzle and mounted onto an extrusion bioprinter. After calibrating the build plate and Z-offset, a 10–15 mm filament purge was performed to ensure stable flow, followed by printing at a constant extrusion rate of 0.06 mL min^{-1}. Constructs were immediately photocrosslinked after deposition using 405 nm light (10 mW cm^{-2}, 60 s) to establish covalent networks. The κ-carrageenan support was then gently rinsed away with PBS. To mimic the lamellar structure of the native cornea, a core GelMA/HAMA layer was first printed and crosslinked, followed by an outer layer with infill orientation rotated by 180° relative to the core. The second layer was subsequently photocured to form a full-thickness, stratified corneal analog. Final printed grafts were rinsed with PBS and stored fully hydrated to maintain structural geometry until further use.

2.9. Suturing ability

The surgical handling potential of the bioengineered cornea was evaluated qualitatively. A cornea-shaped construct was 3D-printed from the GelMA/HAMA precursor and photocrosslinked (405 nm, 10 mW cm^{-2}, 60 s). After equilibration in PBS at 37°C for 24 h, a 9-0 polypropylene suture was passed through the full thickness of the construct, 3 mm from its edge, using a standard curved needle. The suture track was then visually examined for any gross tearing or crack propagation. The absence of such damage was documented as an indicator of the construct's basic robustness and surgical handleability. This test was designed as a qualitative assessment of handling characteristics during a simulated suturing procedure, not

as a quantitative measure of suture retention strength or a direct comparison to native human corneal tissue.

2.10. Swelling and degradation

The hydration capacity and network stability of the printed corneal constructs were evaluated through swelling and degradation studies. For swelling tests, constructs were photopolymerized under 405 nm light and then lyophilized to a constant weight to determine the dry mass (W_d). The samples were immersed in PBS (pH 7.4, 37°C) and weighed (W_s) at predefined intervals until mass equilibrium was reached. The swelling ratio was calculated as shown in **Equation (4).**

$$Swelling\ ratio(\%) = \frac{W_s + W_d}{W_d} \times 100\% \quad (4)$$

The optical transmittance of the fully hydrated constructs was measured after swelling equilibrium across 380–800 nm using a UV–vis spectrophotometer and reported as percent transmission. The dimensional stability of the swelled constructs was assessed using a corneal topographer to measure the anterior corneal curvature and diameter.

For degradation studies, identical hydrogel discs were weighed (W_0) after preparation and incubation in PBS or PBS supplemented with 10 U mL^{-1} collagenase II at 37°C. At scheduled time points, the samples were rinsed, blotted dry, and weighed (W_t). The degradation rate (D) was calculated as shown in **Equation (5).**

$$D(\%) = \frac{W_0 - W_t}{W_0} \times 100\% \quad (5)$$

Data from both swelling and degradation studies are presented as mean ± SD, obtained from three independent samples per condition.

2.11. Tensile and suture retention characterization

Precursor solutions of GelMA, HAMA, and GelMA/HAMA hydrogels were sterile-filtered (0.22 μm), mixed with LAP (0.3% w/v), and cast into silicone strip molds (25 mm × 4 mm × 1.0 mm). The samples were photocrosslinked under 405 nm light (10 mW cm^{-2}, 60 s) and equilibrated in PBS (pH 7.4) at 37°C for 24 h. Before testing, the width and thickness of each sample were measured at three locations and averaged.

For uniaxial tensile testing, hydrated specimens were tested in a temperature-controlled chamber (37°C) using a universal testing machine with a 100 N load cell and pneumatic grips with rubber-faced jaws. Samples were secured at an initial gauge length of 10 mm. Tensile extension was performed at 10 mm min^{-1}. Engineering stress (σ) and strain (ε) were calculated as in **Equations (6)** and **(7).**

$$\sigma = \frac{F}{A_0} \quad (6)$$

$$\varepsilon = \frac{\Delta L}{L_0} \quad (7)$$

where F is the instantaneous force, A_0 is the original cross-sectional area, ΔL is the change in length, and L_0 is the initial length. Young's modulus (E) was then determined from the linear region of the stress–strain curve (0–10% strain). The ultimate tensile strength and failure strain were defined as the peak stress and corresponding strain at rupture, respectively.

For the suture retention test, equilibrated hydrogels were sutured with a 9-0 nylon monofilament using a single stitch placed 2.0 mm from the edge with a 1.0 mm bite. A square knot was tied, leaving 5 mm tails. The suture loop was attached to the upper grip, and the sample was secured in the lower grip, ensuring the pulling direction was perpendicular to the suture line. Specimens were pulled at a constant rate of 5 mm min^{-1} until failure. The peak load was recorded as the suture retention strength and was normalized by sample thickness (N mm^{-1}). For each hydrogel formulation, five strips were tested in uniaxial tension (n = 5), and five independent sutured constructs were evaluated for suture retention (n = 5).

2.12. Burst pressure testing

Disc-shaped samples of GelMA/HAMA composite hydrogels (diameter: 12–14 mm; hydrated thickness 0.50 ± 0.02 mm) were prepared by photocuring and equilibrated in PBS at 37°C for at least 2 h. Each disc was mounted in a two-piece circular fixture with a silicone O-ring, defining a circular test area with an inner diameter of 10 mm. The outlet of the fixture was connected via tubing to a digital pressure sensor (MD-S260, Moekon Sensor Technology Co., Ltd., China) with 0–100 ± 0.1 kPa accuracy, with a syringe serving as the hydraulic pressure source and the entire system filled with PBS. After zeroing the sensor and purging air, the pressure was increased steadily at 1–2 kPa s^{-1}. The burst pressure was recorded as the peak value preceding the first abrupt drop or sustained leak,

preventing further pressurization. Results are expressed as mean ± standard deviation (n = 5). Any tests showing clamp slippage, sample edge tearing, or seal failure were excluded from the analysis.

2.13. Cellular viability assay

The three hydrogel formulations were cast into the bottom of 24-well plates under aseptic conditions and photocrosslinked under 405 nm blue light. The resulting hydrogels were rinsed with sterile PBS to remove unreacted components, then equilibrated in their respective culture media for 24 h. Corneal epithelial cells, stromal fibroblasts, and endothelial cells were seeded onto the hydrogel surfaces at a density of 5×10^4 cells cm^{-2} and incubated at 37°C with 5% carbon dioxide (CO_2). At predetermined time points (Days 1, 3, 5, and 7), the culture medium was replaced with a fresh medium containing 10% (v/v) cell counting kit (CCK)-8 solution. After incubation for 1 h, the absorbance of the CCK-8 solution was measured at 450 nm using a microplate reader (YP-96-1, U-Unip, China) to quantify cellular viability and proliferation. Each condition was tested in three independent wells per time point. Absorbance values are presented as mean ± SD.

To investigate the chemoattractive potential of the biomimetic hydrogel, a Transwell-based coculture assay was established. Sterilized GelMA/HAMA hydrogel precursor was cast into the upper chamber of Transwell inserts (8 μm pore size) to form a thin barrier layer and photocrosslinked. The hydrogel-coated inserts were then equilibrated for 24 h in Dulbecco's Modified Eagle Medium (DMEM)/F-12 medium (VivaCell, China) supplemented with 10% fetal bovine serum (FBS) and 1% penicillin–streptomycin. A chemoattractant gradient was established by adding DMEM/F-12 medium with 10% FBS to the lower chamber. Corneal epithelial cells, stromal fibroblasts, or endothelial cells, suspended in a low-serum medium (DMEM/F-12 with 1% FBS), were seeded onto the surface of the hydrogel in the upper chamber at a density of 5×10^4 cells cm^{-2}. The plates were incubated for 5 days at 37°C under 5% CO_2. After incubation, noninvading cells remaining on the top surface of the hydrogel were carefully removed using a cotton swab. The cells that had invaded into and through the hydrogel layer were then fixed with 4% paraformaldehyde, stained with 0.1% (w/v) crystal violet, and imaged under a bright-field microscope (MSD-S820, Murzider, China). Quantitative analysis was performed by calculating the percentage of the total area occupied by the stained, invaded cells across multiple predefined fields of view. Three independent inserts were analyzed per condition.

2.14. Cell-laden bioprinting and fluorescent imaging

Primary mouse corneal stromal cells (P3–P4; iCell Bioscience, China) were harvested, counted, and resuspended in a sterile GelMA/HAMA prepolymer solution containing 0.30% (w/v) LAP at a density of 5×10^6 cells mL^{-1}. The cell–bioink mixture was gently mixed at 37°C and maintained at this temperature. A granular κ-carrageenan support bath (8–10 mm depth) was autoclave-sterilized and equilibrated to 15°C. The stromal cell-laden bioink was loaded into a sterile 5 mL syringe equipped with a 160 μm nozzle, mounted on an extrusion bioprinter, and purged (10–15 mm) to stabilize flow. Following the protocol in **Section 2.8**, the stromal core was printed directly into the support bath using a layer height of 160 μm and a 100% concentric infill pattern under constant volumetric extrusion (0.06 mL min^{-1}; print and travel speeds of 60 and 80 mm s^{-1}, respectively). Constructs were immediately photocrosslinked (405 nm, 10 mW cm^{-2}, 60 s), after which the κ-carrageenan support was dissolved and carefully rinsed away with PBS.

For the epithelial layer, primary mouse corneal epithelial cells (P3–P4) were suspended in fresh GelMA/HAMA/LAP prepolymer at 3×10^6 cells mL^{-1} and processed identically. The printed stromal graft was rotated 180°, and the epithelial bioink was deposited onto its outer surface and photocured (405 nm, 10 mW cm^{-2}, 60 s). Finally, primary mouse corneal endothelial cells (P3–P4) were seeded onto the inner (posterior) surface via repeated pipette dripping (2–3 passes at 4×10^5 cells cm^{-2}) onto the pre-equilibrated hydrogel surface. After a 20–30-min attachment period at 37°C, the graft was gently rinsed with PBS. The bioprinted corneal equivalents were maintained in DMEM/F-12 medium and incubated at 37°C in a humidified 5% CO_2 atmosphere.

After 2 days of culture, constructs were rinsed with PBS and incubated in a solution containing 2 μM calcein-acetoxymethyl ester and 4 μM ethidium homodimer-1 for 40 min at 37°C to assess cell viability. The stained constructs were then imaged using a confocal microscope (STELLARIS 5, Leica, Germany). After 7 days of culture, samples were fixed in 4% paraformaldehyde and permeabilized with 0.1% Triton X-100. They were then stained with fluorescein isothiocyanate (FITC)-phalloidin for 60 min to visualize F-actin, washed three times with PBS, counterstained with 4',6-diamidino-2-phenylindole (DAPI) to label nuclei, and imaged by confocal microscopy to assess cell distribution and structural integrity.

2.15. 3D confocal imaging of the bioprinted cornea

The spatial organization of cells within the 3D-bioprinted corneal constructs was visualized using multiplex immunofluorescence staining and confocal microscopy.

The constructs, comprising epithelial, stromal, and endothelial layers, were fixed, stained, and imaged as follows: The 3D-bioprinted corneal constructs were washed with PBS and immobilized in a 24-well plate for processing. They were then fixed with a 4% paraformaldehyde and 0.25% glutaraldehyde solution at room temperature for 45 min, followed by three 5-min washes with PBS. We then permeabilized the constructs with 0.5% Triton X-100 in PBS for 30 min and subsequently blocked with 3% BSA in PBS for 1 h at room temperature. For multiplex immunofluorescence staining, the constructs were incubated overnight at 4°C with a mixture of the following primary antibodies diluted in 3% BSA/PBS: anticytokeratin 18 (647-conjugated, 1:200 dilution; 10830-1-AP, Proteintech, China) to label epithelial cells and anti-ATP1A1 (FITC-conjugated, 1:200 dilution; 14418-1-AP, Proteintech, China) to label endothelial cells. After incubation, the constructs were washed three times with PBS for 5 min each. Following the primary antibody staining, the constructs were incubated with CoraLite-labeled Phalloidin (1:500 dilution; PF0003, Proteintech, China) for 30 min at room temperature to label F-actin in stromal cells. Finally, all samples were counterstained with DAPI for 10 min to visualize nuclei and washed thoroughly with PBS. The stained constructs were imaged using a confocal microscope. The following excitation/emission settings were used: cytokeratin 18 (647 nm/pink), phalloidin (594 nm/red), ATP1A1 (488 nm/green), and DAPI (405 nm/blue). Z-stacks were acquired to capture the full 3D structure of the constructs. All staining and imaging procedures were performed on three independently fabricated constructs ($n = 3$). For each construct, at least three nonoverlapping fields of view were imaged per channel.

2.16. Gene expression analysis in corneal cells by quantitative polymerase chain reaction

To evaluate the gene expression profiles of corneal cells cultured on different hydrogel substrates, corneal epithelial, stromal, and endothelial cells were seeded at a density of 5×10^5 cells mL^{-1} within GelMA, HAMA, and GelMA/HAMA hydrogels. After the culture period, total RNA was extracted directly from the cell-laden hydrogels using the High Purity RNA Extraction Kit (Q20802, TransGen Biotech, China). Genomic DNA was removed, and first-strand cDNA was synthesized from the purified RNA using the TransScript One-Step gDNA Removal and cDNA Synthesis SuperMix kit (AT311, TransGen Biotech, China) according to the manufacturer's instructions. Quantitative PCR (qPCR) was performed using the PerfectStart Green qPCR SuperMix (AQ601, TransGen Biotech, China) on a real-time qPCR system. *Actb* (β-actin) was used as the reference gene for normalization, and reactions were performed using gene-specific primers (sequences listed in **Table S1**). Relative gene expression levels were calculated using the $2^{-\Delta\Delta Ct}$ method. For each cell type and hydrogel condition, RNA was isolated from three independent biological replicates ($n = 3$), with each sample assayed in technical triplicate. Gene expression data are presented as mean ± SD.

2.17. Statistical analysis

All statistical analyses were performed using Statistical Package for Social Sciences (SPSS 20.0, IBM, USA) and GraphPad Prism (version 9.5.1, Dotmatics, UK). Data are presented as mean ± SD. Group comparisons were carried out using one-way analysis of variance, followed, where appropriate, by Tukey's honestly significant difference post hoc test. Homogeneity of variances was assessed with Levene's test. Unless otherwise stated, all tests were two-sided with a significance level of $\alpha = 0.05$. Statistical significance is indicated as $^*p < 0.05$, $^{**}p < 0.01$, and $^{***}p < 0.001$. For analyses involving multiple hypotheses, p-values were adjusted using the Benjamini–Hochberg procedure to control the false discovery rate. Sample sizes (n) for each experiment are reported in the corresponding figure legends.

3. Results

3.1. Synthesis and characterization of the gelatin methacryloyl/hyaluronic acid methacryloyl hydrogel

The UV-curable, temperature-sensitive GelMA/HAMA composite hydrogel, consisting of 10% (w/v) GelMA, 1% (w/v) HAMA, and 0.3% (w/v) LAP, was designed as a corneal scaffold to enable embedded bioprinting, as detailed in our previous reports.[24] GelMA and HAMA were synthesized by reacting gelatin and hyaluronic acid with MA, with methacrylation degrees of 73.6 ± 0.3% and 13.7 ± 0.1%, respectively (Figure S1). While GelMA provides a supportive scaffold for corneal cell growth, the incorporation of HAMA aims to modulate key physical characteristics relevant to corneal function. Contact angle measurements revealed that GelMA hydrogel exhibited a high contact angle (>84°), indicating a relatively hydrophobic surface (Figure 2A and B). In contrast, the HAMA hydrogel showed a markedly lower contact angle (< 25°), attributable to its abundance of hydroxyl and carboxyl groups that enhance water affinity. The GelMA/HAMA hydrogel presented an intermediate contact angle (~50°) closer to the wettability range of the native cornea (55–65°).[25] Optical characterization across the visible spectrum (380–780 nm) demonstrated that the GelMA/HAMA composite hydrogel achieved moderate optical clarity, with transmittance increasing

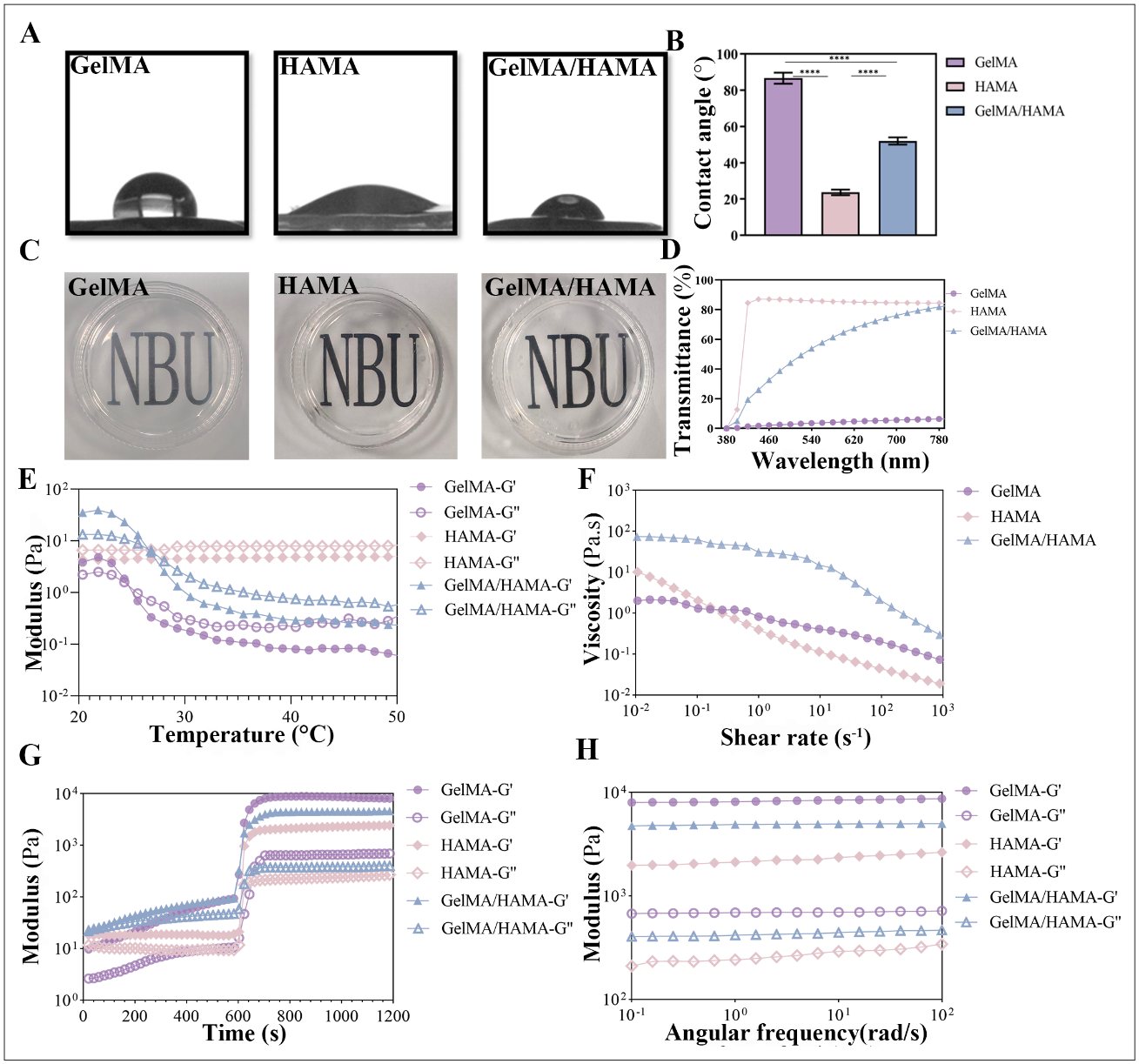

Figure 2. Rheological and physicochemical characterization of GelMA, HAMA, and GelMA/HAMA hydrogels. (A) Representative sessile-drop contact-angle images on hydrogel surfaces. (B) Contact angle (°; $n = 3$). (C) Macroscopic appearance of hydrated samples at identical thickness. (D) Ultraviolet–visible transmittance spectra across 380–780 nm; $n = 3$). (E) Temperature sweep (20–50°C) monitoring the gel–sol transition. (F) Shear-flow ramp at 37°C (0.01–100 s^{-1}) revealing zero-shear viscosity and shear-thinning behavior. (G) Time-sweep monitoring of storage (*G'*) and loss (*G"*) moduli during photocrosslinking (405 nm irradiation initiated at 600 s). (H) Frequency sweep of photocrosslinked hydrogels. For panel (B), statistical comparisons among hydrogels were performed using one-way analysis of variance. Note: ****$p < 0.0001$. Abbreviations: GelMA: Gelatin methacryloyl; HAMA: Hyaluronic acid methacryloyl.

from approximately 30% at 400 nm to around 80% at longer wavelengths (Figure 2C and D). This performance represents a substantial improvement over GelMA alone (<20% transmittance), though it remains lower than that of the highly transparent HAMA hydrogel (> 90%). Collectively, the transmittance spectrum of 30–80% positions the composite as an optically promising, yet not native-equivalent, material for corneal scaffold applications, effectively balancing transparency with other essential properties.

The temperature sensitivity and UV-curable gelation of GelMA/HAMA composites used as bioprinting inks were analyzed through rheological measurements. As shown in Figure 2E, both GelMA and GelMA/HAMA precursors

underwent gel–sol transitions at 24 and 27°C, respectively, while HAMA maintained a relatively stable modulus across the entire temperature range. The stiffness of the GelMA/HAMA gels formed below 27°C was found to be greater than that of both GelMA and HAMA, whereas the modulus of the sol state above 27°C fell between the values of GelMA and HAMA. This reversible, temperature-mediated sol–gel transition facilitates smooth flow extrusion during printing. Moreover, the rapid formation of high-modulus gels ensures the stability and fidelity of the printed structures. Additionally, the GelMA/HAMA precursors at 37°C exhibited shear-thinning behavior (Figure 2F), improving the printability of the inks under lower shear stress, thereby protecting cell viability during cell-laden bioprinting.

Upon UV initiation, the GelMA/HAMA composite rapidly transformed from a thermosensitive soft gel into a covalently crosslinked hydrogel with a storage modulus of 4,497 Pa, exceeding that of the HAMA hydrogel but remaining lower than that of the GelMA (Figure 2G). Moreover, frequency-sweep analyses showed that the loss modulus of the GelMA/HAMA hydrogel increased slightly with frequency, while the storage modulus remained nearly constant (Figure 2H). These results indicate that incorporating HAMA into GelMA yields a mechanically robust yet compliant network, which is advantageous for maintaining shape fidelity in curved corneal bioprinting. Tensile tests demonstrated that GelMA, HAMA, and GelMA/HAMA hydrogels all exhibited failure stresses of 250–300 kPa (Figure S2), with the composite showing performance comparable to GelMA. In *ex vivo* suturing tests, the constructs maintained mechanical integrity, exhibiting only localized softening around the suture site without macroscopic tearing. These results support good handling characteristics and resistance to suture-induced damage under experimental conditions. Consistently, burst-pressure tests yielded a mean failure pressure of 11.4 ± 0.31 kPa (Figure S3), which is several times the physiological intraocular pressure and falls within the lower range of experimental corneal sealants. These results suggest that the GelMA/HAMA hydrogel provides sufficient short-term pressure retention, though further improvements are needed to achieve more stringent mechanical performance requirements.

3.2. Embedded printing of the 3D corneal constructs

To fabricate curved corneal constructs with high geometric fidelity via embedded micro-extrusion printing, we employed a sacrificial support bath composed of a κ-carrageenan microgel suspension, optimized based on our previous work.[26,27] A 0.4% κ-carrageenan suspension was selected, as it demonstrated suitable yield stress, pronounced shear-thinning, and rapid self-healing properties at the printing temperature (Figure 3B and C). These rheological characteristics are essential for supporting the deposition and shape retention of fine, curved filaments without causing structural collapse. A 3D corneal model was designed in Rhino with the following dimensions: an outer radius of curvature of 7.8 mm, an inner radius of curvature of 6.8 mm, a transverse diameter of 11.0 mm, a longitudinal diameter of 10.0 mm, and a central thickness of 0.5 mm (Figure 3C). When the GelMA/HAMA ink was extruded through a 160 μm inner-diameter nozzle into this support bath, the deposited filaments rapidly underwent physical gelation upon cooling to the ambient temperature of the bath (Figure 3D). After printing, the entire structure was photocrosslinked under UV light and then gently extracted from the κ-carrageenan support. The obtained hydrogel corneal scaffold accurately replicated the curvature and dimensions of the original digital model.

Suturing is a fundamental procedure in corneal surgery. To assess the handling characteristics and structural robustness of the GelMA/HAMA corneal scaffold in a simulated surgical context, we performed a qualitative suturing test. Eight evenly spaced stitches were placed circumferentially using ophthalmic-grade 9-0 polypropylene sutures. As shown in Figure 3E, the scaffold maintained its structural integrity throughout the procedure, resisting macroscopic tearing or significant deformation at the suture sites. This result demonstrates the scaffold's ability to withstand basic surgical manipulation *in vitro*, indicating favorable handling characteristics for potential use in ophthalmic tissue engineering research. This excellent suture retention property can be linked to the balanced mechanical stability and flexibility inherent to the GelMA/HAMA composite hydrogels.

3.3. *In vitro* swelling and degradation of gelatin methacryloyl/hyaluronic acid methacryloyl corneal constructs

The controlled swelling behavior and degradation of scaffolds are crucial for surgical success and postoperative recovery. An ideal corneal scaffold must exhibit minimal swelling (<10%) to maintain optical clarity and structural stability, while demonstrating controlled degradation kinetics synchronized with corneal regeneration (4–8 weeks). The swelling and degradation properties of the GelMA/HAMA corneal scaffolds were systematically evaluated to assess their suitability for corneal applications. As shown in Figure 3F, the scaffolds demonstrated optimal water absorption characteristics in PBS (pH 7.4), reaching an equilibrium swelling ratio of 9.11 ± 0.48% within 360 min. This relatively low swelling was consistent with preservation of moderate optical transmittance across the visible spectrum before and after hydration (Figure 3G).

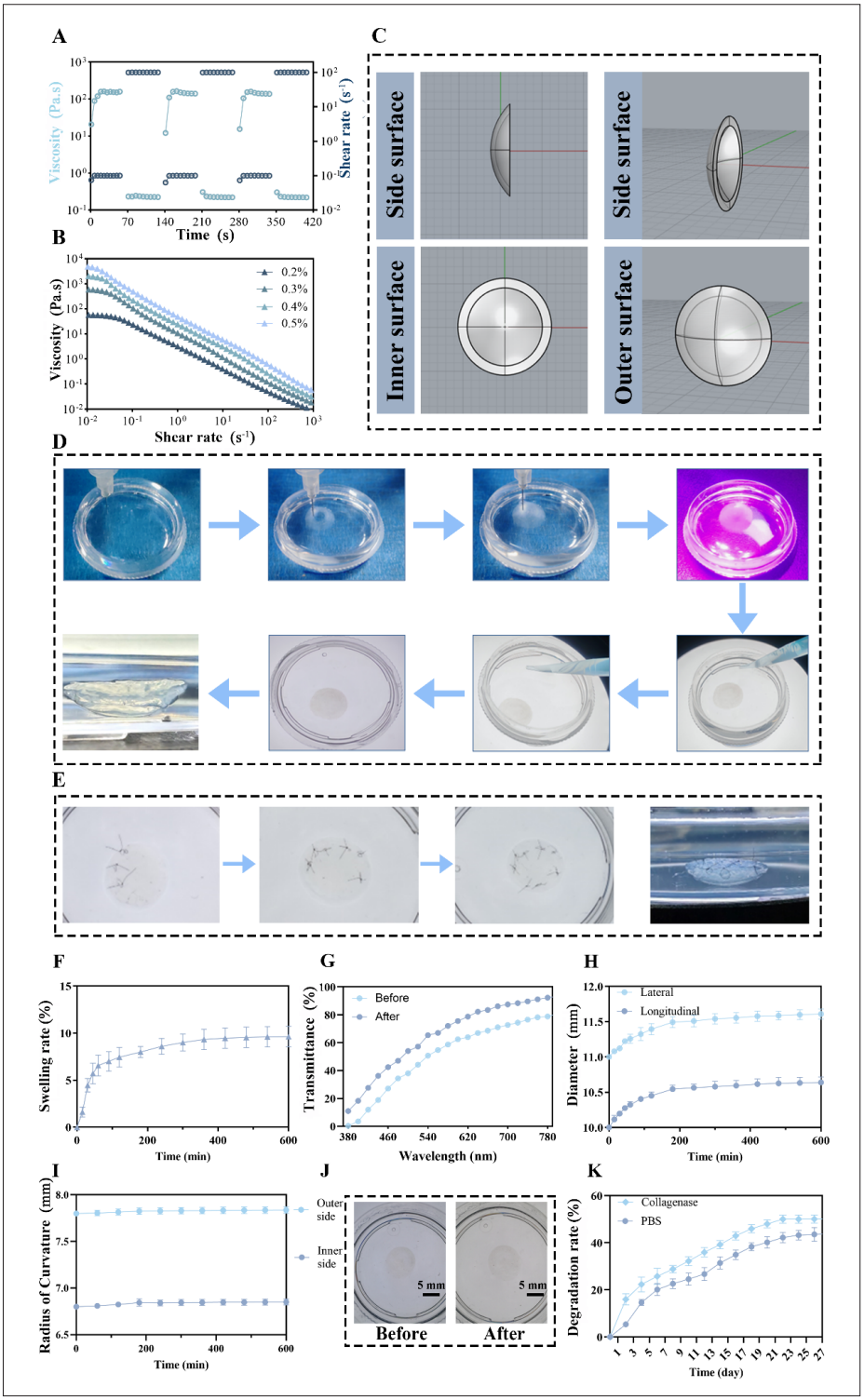

Figure 3. Rheological properties, fabrication process, and structural stability of the bioengineered corneal scaffold. (A) Self-healing behavior of the κ-carrageenan support bath under alternating shear. (B) Shear-thinning flow behavior of κ-carrageenan at varying concentrations. (C) Computer-aided design model illustrating corneal geometry and curvature. (D) Sequential bioprinting process for scaffold fabrication. (E) Suture retention test demonstrating surgical feasibility. (F) *In vitro* degradation profiles in phosphate-buffered saline (PBS) and collagenase environments. (G) Optical transmittance before and after swelling (mean ± standard deviation [SD], $n = 3$). (H) Temporal changes in lateral and longitudinal dimensions during hydration (mean ± SD, $n = 3$). (I) Evolution of outer and inner curvature radii during hydration (mean ± SD, $n = 3$). (J) Macroscopic view of scaffolds before and after hydration. Scale bar: 5 mm. (K) Enzymatic degradation in collagenase compared to PBS control (mean ± SD, $n = 3$).

The hydrated constructs also maintained dimensional stability, with the outer curvature radius remaining below 7.9 mm, the inner curvature radius below 6.9 mm, the transverse diameter below 11.59 mm, and the longitudinal diameter below 10.6 mm (Figure 3H and I).

Degradation studies were performed under both passive (PBS only) and enzymatic (collagenase II, 10 U mL^{-1}) conditions to model different aspects of *in vivo* breakdown. In PBS at 37°C, the GelMA/HAMA scaffolds showed a gradual degradation profile with 44.22 ± 0.37% mass retention after 28 days, following near-linear kinetics. In collagenase solution, the scaffolds exhibited bioresponsive degradation behavior. They maintained structural integrity during the critical initial 2-week epithelialization period (≤ 39.55% mass loss) and subsequently accelerated degradation (50.46 ± 0.17% total mass loss at the 4th week). This enzyme-responsive degradation profile suggests that the scaffold's stability could be modulated by local proteolytic activity. Overall, the observed minimal swelling supports the scaffold's potential to maintain dimensional and optical consistency in an aqueous environment, while the tunable degradation kinetics in collagenase indicate a capacity for cell- or enzyme-mediated remodeling. These *in vitro* properties are consistent with initial requirements for a corneal stromal scaffold, though their functional relevance must be further evaluated in biological systems.

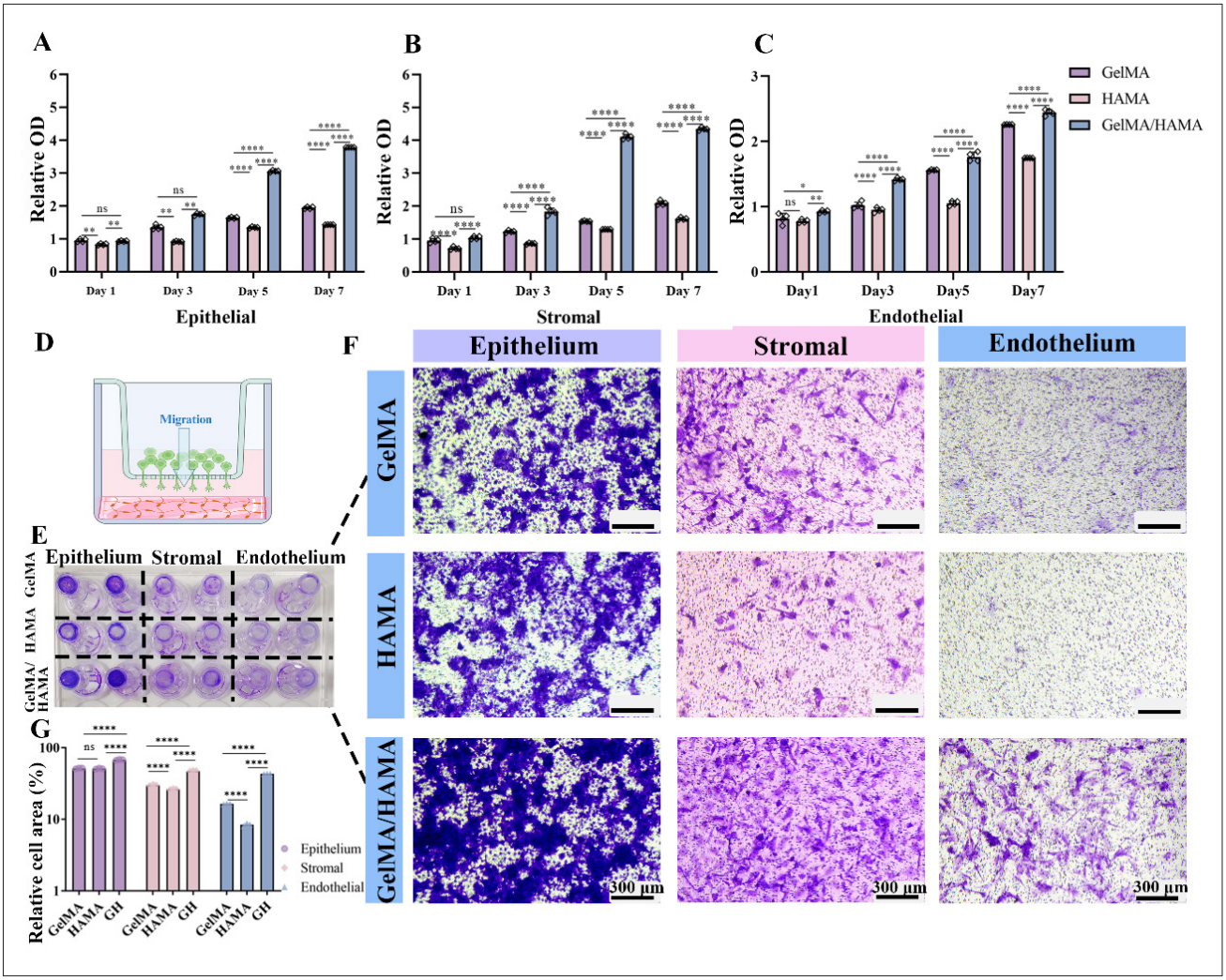

Figure 4. Cell viability and migration of corneal cells on hydrogel substrates. (A–C) Viability of corneal epithelial (A), stromal (B), and endothelial (C) cells on GelMA, HAMA, and GelMA/HAMA hydrogels measured by Cell Counting Kit-8 assay at designated time points (mean ± standard deviation [SD], $n = 3$). (D) Schematic illustration of the Transwell migration assay. (E) Representative images of the Transwell assay setup. (F) Micrographs of migrated cells on the underside of the membranes. 20×. (G) Quantification analysis of cell migration, presented as the percentage of area covered by migrated cells (%, mean ± SD, $n = 3$). For panels (A–C, G), group differences were analyzed by one-way analysis of variance with Tukey's honestly significant difference post hoc test. Notes: ns, not significant; $^{*}p < 0.05$; $^{**}p < 0.01$; $^{****}p < 0.0001$.

3.4. Proliferation and migration of corneal cells on gelatin methacryloyl/hyaluronic acid methacryloyl hydrogels

The cytocompatibility of GelMA/HAMA hydrogels was evaluated by culturing corneal epithelial, stromal, and endothelial cells on their surfaces, using single-component GelMA and HAMA hydrogels as controls. Cell viability and proliferation were assessed via CCK-8 assay at Days 1, 3, 5, and 7. As illustrated in Figure 4A, the optical density (OD) values of corneal epithelial cells on Days 1 and 3 were comparable across all hydrogel groups. However, by Days 5 and 7, corneal epithelial cells demonstrated a significantly higher proliferation rate on the GelMA/HAMA composite hydrogels compared to those on the GelMA and HAMA hydrogels. For corneal stromal and endothelial cells, the OD value on the composite hydrogels was significantly greater than on HAMA hydrogels as early as Day 1. This trend continued through Days 3–7, with marked increases in proliferation observed by Day 5 relative to both HAMA and GelMA hydrogels (Figure 4B and C). These results showed that corneal epithelial cells exhibited a lower proliferation rate on the composite hydrogel substrate relative to stromal and endothelial cells. Notably, the relative OD values for all three cell types on the composite hydrogels on Days 5 and 7 were similar, suggesting the onset of contact inhibition, a characteristic of normal cell growth behavior. Collectively, these findings demonstrate that the GelMA/HAMA composite hydrogel provides a highly cytocompatible substrate that supports robust, coordinated proliferation of key corneal cell types.

To assess the chemotactic response of corneal cells to the printed scaffolds, we performed a Transwell-based migration assay (Figure 4D). Hydrogel samples were placed in the lower chamber, and cells were seeded in the upper chamber. After 24 h, cells that had migrated to the underside of the membrane were stained and quantified. As illustrated in Figure 4G, the GelMA/HAMA hydrogel supported the most pronounced directional migration toward the hydrogel-containing lower compartment, followed by GelMA and then HAMA, demonstrating that cell migration is guided by material-specific biochemical cues. Quantitative analysis further revealed that the GelMA/HAMA composite hydrogel significantly enhanced cell spreading area compared to single-component hydrogels. Notably, endothelial cells exhibited the strongest response, with a 5.17 ± 0.29-fold increase compared to HAMA. These results suggest that the GelMA/HAMA composite presents biochemical or physical cues that promote corneal cell migration in this *in vitro* assay.

3.5. 3D bioprinted multilayered cell-laden corneal constructs

The favorable rheological properties, biocompatibility, and ability to support corneal cell proliferation and migration make GelMA/HAMA a suitable bioink for fabricating cell-laden constructs. To create a trilaminar biomimetic structure, we printed a stromal layer by extruding GelMA/HAMA bioink laden with corneal stromal cells. After 24 h of culture, live/dead cell staining revealed that the stromal cells maintained robust viability of 93% (Figure 5A). Furthermore, after 48 h, 80% of the cells had spread and formed pseudopodia within the 3D culture matrix (Figure 5B). These observations confirm that the GelMA/HAMA hydrogel provides a conducive 3D microenvironment for stromal cell survival and early integration.

Given the differential proliferation rates observed for epithelial and endothelial cells on the hydrogel surface, we adopted a sequential bioprinting and seeding strategy to assemble the full-thickness construct (Figure 5C). Corneal epithelial cell-laden hydrogels were first printed onto the anterior surface of the printed stromal layer. After 24 h of culture to allow for initial epithelial growth, corneal endothelial cells were seeded onto the posterior surface. Following an additional 48 h of culture, the constructs were immunostained for cytokeratin 18 (epithelium), ATP1A1 (endothelium), F-actin (stromal cytoskeleton), and nuclei. Confocal imaging revealed that epithelial, stromal, and endothelial cells were distributed in spatially distinct layers, recapitulating the trilaminar organization of the cornea (Figure 5D).

To evaluate the structural stability of the layered architecture, we extended the culture period and conducted layer-resolved confocal imaging of the same trilayer constructs on Days 7 and 14 (Figure S4). Whole-mount and high-magnification images confirmed the maintenance of distinct cellular strata throughout the culture period. The epithelial layer formed a dense, continuous covering on the anterior surface; the stromal region developed a highly organized, fibrillar extracellular matrix; and the endothelial layer remained as a confluent, polygonal monolayer on the posterior side. Importantly, this stratified epithelial–stromal–endothelial organization remained intact throughout the 14-day culture, with no signs of delamination or substantial loss of coverage. These results demonstrate that the printed corneal equivalents maintain their layer-specific architecture over relevant timeframes. The sustained structural fidelity of the constructs underscores the capability of the GelMA/HAMA hydrogel scaffold in replicating the native, multilayered organization of the cornea.

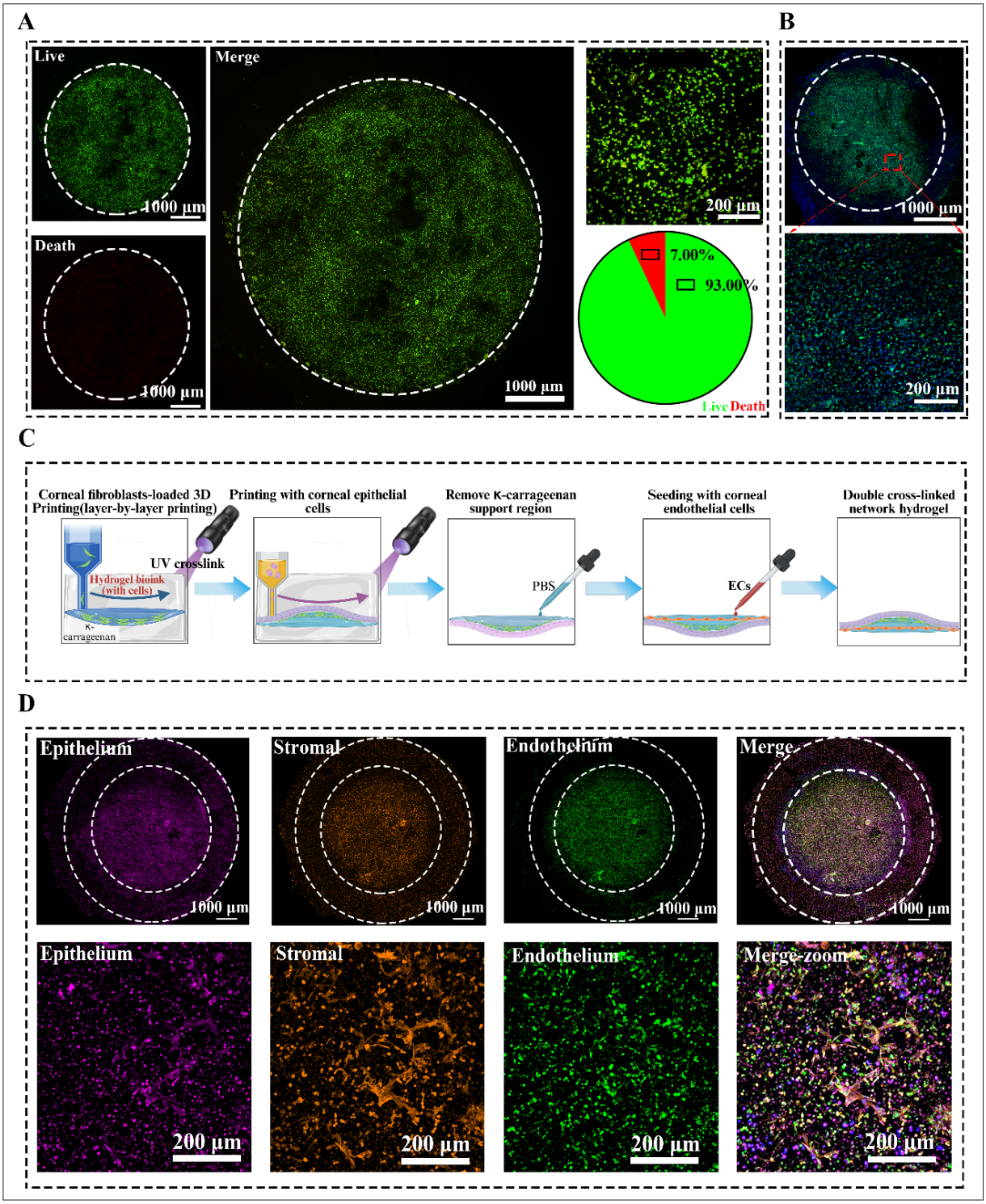

Figure 5. Cell viability and morphology of a trilaminar, cell-laden bioengineered cornea. (A) Confocal live/dead micrographs of the printed construct showing high cell viability. Scale bars: whole-mount (X-Y tiled): 10×, 1,000 μm; representative field of view (FOV): 10×, 200 μm. (B) Confocal visualization of the cytoskeletal architecture within the cell-laden corneal construct, with whole-mount and region-of-interest zooms. Scale bar: whole-mount (X-Y tiled): 1,000 μm, representative FOV: 10×, 200 μm. (C) Schematic diagram of the biofabrication process: embedded printing of a keratocyte-laden stromal layer; UV crosslinking; deposition of epithelial cells; removal of the κ-carrageenan support bath; seeding of ECs, and formation of the final composite hydrogel construct. (D) Confocal micrographs of the multilayered construct showing epithelial, stromal, and endothelial layers with a merged view and high-magnification insets; the outer circle indicates the construct boundary. Scale bars: whole-mount (X-Y tiled): 10×, 1,000 μm, representative FOV: 10×, 200 μm. Abbreviations: Ecs: Endothelial cells; PBS: Phosphate-buffered saline; UV: Ultraviolet.

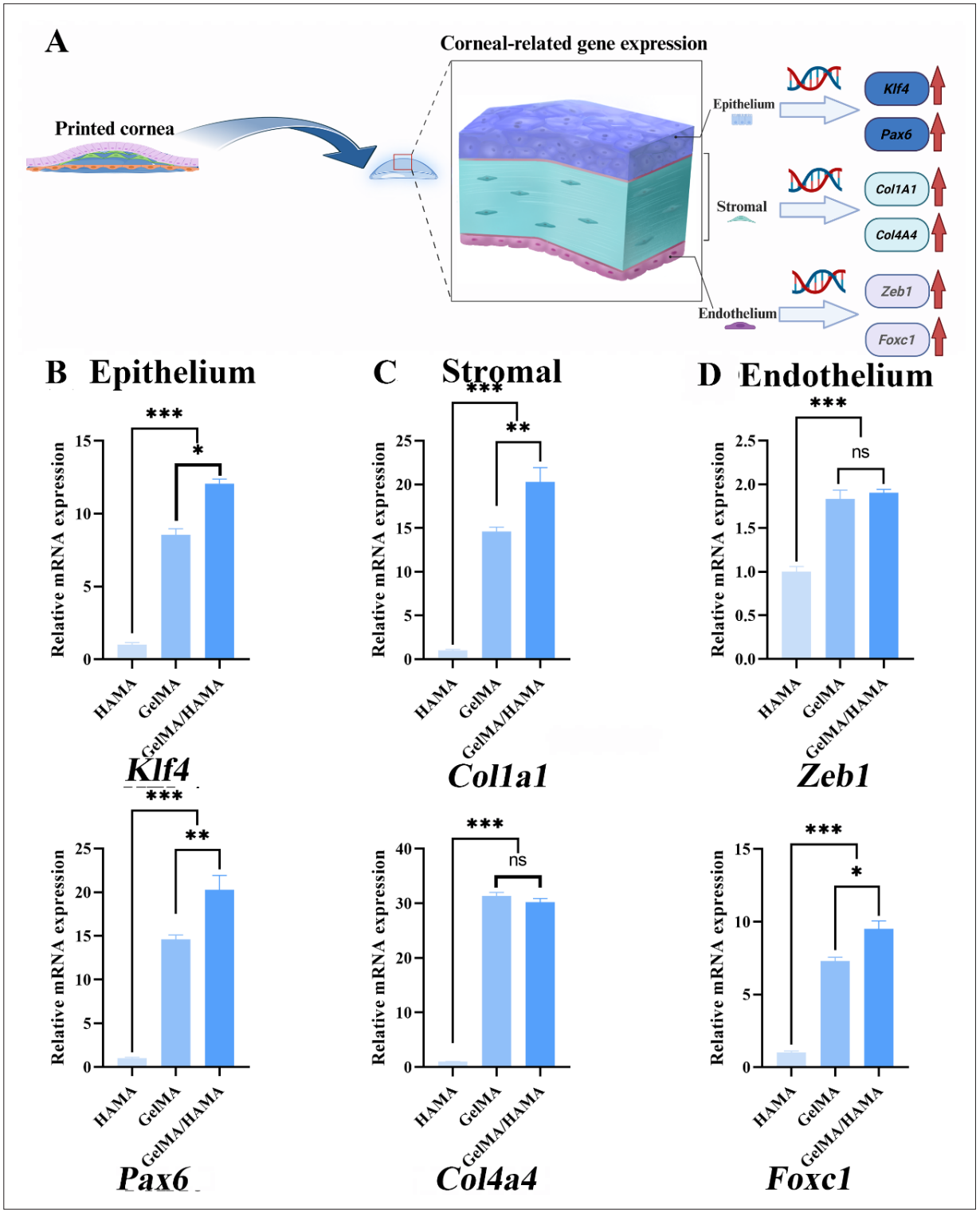

Figure 6. Layer-specific expression of corneal lineage markers in a 3D bioengineered cornea. (A) Schematic of postculture sampling and qPCR workflow for the printed construct. (B,D) Relative mRNA expression of (B) epithelial identity genes (*Klf4*, *Pax6*), (C) stromal extracellular matrix genes (*Col1a1*, *Col4a4*), and (D) endothelial-associated markers (*Zeb1*, *Foxc1*) on hyaluronic acid methacryloyl (HAMA), gelatin methacryloyl (GelMA), and GelMA/HAMA hydrogels. Data are shown as mean ± standard deviation (SD) from $n = 3$ biological replicates. Group differences were assessed by one-way analysis of variance with Tukey's honestly significant difference post hoc test. The p-values were adjusted for multiple testing using the false discovery rate. Notes: ns, not significant; $^{*}p < 0.05$; $^{**}p < 0.01$; $^{***}p < 0.001$.

3.6. Gene expression analysis in the 3D-bioprinted biomimetic cornea

To evaluate the phenotypic development of cells within the bioprinted construct, real-time qPCR was performed on distinct cell layers after 72 h of culture (Figure 6A). Gene expression levels were normalized to the housekeeping gene *Actb* (β-actin). In the epithelial layer, we observed pronounced upregulation of *Klf4*, which is a barrier-maintenance factor that preserves epithelial homeostasis and restrains epithelial–mesenchymal transition, and *Pax6*, the master regulator of ocular-surface lineage commitment (Figure 6B). Both genes were maximally expressed on the GelMA/HAMA composite (GelMA/HAMA > GelMA >> HAMA), indicating that the hybrid matrix most effectively promotes epithelial differentiation and barrier maturation. Within the stromal compartment, *Col1a1* (fibrillar collagen I) and *Col4a4* (basement membrane–associated collagen IV) were robustly expressed (Figure 6C), following the pattern GelMA/HAMA ≥ GelMA >> HAMA, consistent with active extracellular-matrix production and coordinated collagen I/IV assembly that underpins optical clarity and mechanical cohesion.

In the endothelial layer, transcriptional regulators *Zeb1* and *Foxc1*, which are associated with endothelial identity and junctional organization, were both upregulated compared to the HAMA control (Figure 6D), providing evidence of phenotypic orientation toward an endothelial-like state rather than demonstrating fully mature, functionally equivalent human corneal endothelium. Specifically, *Foxc1* expression was significantly higher in the GelMA/HAMA group than in the GelMA group, while *Zeb1* levels showed no significant difference between these two conditions. These findings indicate that the composite hydrogel promotes an endothelial-like, junction-forming phenotype. Broader temporal qPCR analysis over 3, 7, and 14 days (Figure S5) further indicated that the GelMA/HAMA environment consistently suppressed markers of myofibroblast transition (*Acta2* [α-smooth muscle actin], *Tagln* [transgelin], and *Myl9*) relative to single-component controls, while maintaining or enhancing expression of genes associated with transport and barrier formation (*Aqp1*, *Atp1a1* [Na^+/K^+-ATPase α1], and *Slc4a4* [sodium bicarbonate cotransporter 1]). Furthermore, elevated expression of *Col1a1*, *Mmp2*, and the chemokine receptor *Cxcr4* was observed, suggesting the establishment of a microenvironment conducive to controlled extracellular matrix remodeling and cellular migration. Overall, these results demonstrate that our 3D-bioprinted corneal construct recapitulates key molecular features of the native cornea within 72 h and sustains a pro-regenerative microenvironment over time. This microenvironment coordinately supports epithelial and stromal gene expression programs, promotes an endothelial-like transcriptional profile, and attenuates pathways linked to fibrosis.

4. Discussion

This study presents a proof-of-concept for fabricating a biomimetic corneal scaffold using embedded microextrusion 3D bioprinting of a GelMA/HAMA composite hydrogel. The scaffold partially replicates key structural features of the native cornea, exhibiting moderate yet promising optical transparency in the visible spectrum, experimentally assessed mechanical robustness suitable for *in vitro* handling and suturing, and excellent *in vitro* biocompatibility. The hybrid GelMA/HAMA network established through photopolymerization offers an improved balance among printability, transparency, and support for corneal cell growth compared to reports on single-component hydrogels.[28-30] The tailored rheological properties of the bioink, featuring shear-thinning at 37°C and a reversible sol–gel transition near 27°C, enable high-fidelity printing and cell viability during the "extrude–stabilize–cure" sequence. Subsequent photocrosslinking (405 nm) yields a covalently crosslinked network with a plateau modulus of ~4.5 kPa, which provides sufficient structural integrity for multilayer fabrication while remaining compliant enough to preserve curvature and withstand basic surgical manipulation *in vitro*.

We employed a sequential "epithelial printing–matrix printing–endothelial seeding" strategy to assemble a trilaminar, cell-populated structure. Biologically, the 3D-printed hydrogel matrix supported high cell viability and promoted the expression of molecular characteristics of corneal lineages. Layer-specific qPCR analysis confirmed phenotype-specific maturation across all layers. In the epithelial compartment, coordinated upregulation of *Klf4* and *Pax6* promoted stratified differentiation and cornea-specific keratin expression, consistent with barrier-associated differentiation and a smoother epithelial coverage. Within the stroma, elevated expression of *Col1a1* and *Col4a4* indicates active extracellular matrix synthesis. In the endothelial layer, upregulation of *Zeb1* and *Foxc1*, along with sustained expression of transporters, such as *Aqp1* and *Atp1a1*, suggests the development of an endothelial-like, junction-associated transcriptional profile under these culture conditions.

Taken together, this work establishes an early-stage proof-of-concept for a trilayered GelMA/HAMA-based corneal construct. We have demonstrated controlled structural organization, cytocompatibility with the three principal corneal lineages, and preliminary phenotypic and transcriptional markers indicative of epithelial-, stromal-,

and endothelial-like identities. However, functional performance remains incompletely characterized, and our current evidence is restricted to short-term *in vitro* assays without direct validation of barrier or pump function, or long-term behavior under physiologically relevant ocular surface conditions. Future work should therefore systematically evaluate the material's long-term optical stability in tear film environments, including its behavior under dynamic conditions, such as hydration cycling, protein/lipid adsorption, blink-induced shear stress, and surface wetting energetics. In parallel, establishing a comprehensive immunocompatibility profile will be essential to control potential postimplantation neovascularization and fibrosis, while ensuring durable biocompatibility with both corneal epithelial and endothelial tissues. Finally, 6- to 12-month rabbit corneal injury models can be employed to comprehensively assess postimplantation outcomes, including immune rejection, tissue regeneration capacity, reinnervation efficiency, and tear film dynamics (assessed through tear break-up time, interferometry, and contact angle hysteresis), with benchmarking against current state-of-the-art corneal substitutes. These systematic investigations will be required before this engineered platform can be credibly considered as a candidate to help address the clinical challenges of donor shortage and graft rejection.

5. Conclusion

In summary, this study demonstrates the feasibility of fabricating a trilaminar, cell-laden corneal construct using embedded microextrusion 3D bioprinting with a GelMA/HAMA composite hydrogel. The engineered scaffold recapitulates key structural features of the native cornea and exhibits promising *in vitro* properties, including moderate optical transparency (30–80% across the visible spectrum), a wettability profile suitable for epithelial attachment (contact angle ~50°), minimal swelling (<10%), and controlled degradation kinetics. The scaffold exhibited mechanical robustness sufficient for basic experimental handling, with a burst pressure (~11.4 kPa) exceeding typical physiological intraocular pressure, indicating short-term *in vitro* stability rather than clinical readiness. Furthermore, the printed GelMA/HAMA scaffold supported robust cellular proliferation of corneal epithelial, stromal, and endothelial cells. Gene expression analysis confirmed the phenotypic orientation of these cells toward their respective lineages, evidenced by the upregulation of *Klf4* and *Pax6* in the epithelium, *Col1a1* and *Col4a4* in the stroma, and *Zeb1* and *Foxc1* in the endothelium. Collectively, these results establish this bioprinted, trilayered construct as a solid proof-of-concept model for corneal tissue engineering. This work provides a foundational platform for further *in vitro* studies and sets the stage for subsequent investigations into long-term functional performance.

Acknowledgments

We thank the Core Facilities, Health Science Center of Ningbo University, for their technical support.

Funding

This research was supported by the Science and Technology Innovation 2035 Major Project of Ningbo (No. 2024Z212), the Ningbo Natural Science Foundation (No. 2022J121), Zhejiang Provincial Disease Prevention and Control Science and Technology Program (Grant No. 2025JK276) and the Key Laboratory of Polymeric Composite & Functional Materials of the Ministry of Education (No. PCFM-2025A02).

Conflict of interest

The authors declare that they have no known competing financial interests or personal relationships that could have influenced the work reported in this paper.

Author contributions

Conceptualization: Yang Luo, Hua Zhang, Tong Zhu
Formal analysis: Tong Zhu, Cuicui Su, Lu Yang
Investigation: Tong Zhu, Shengkai Yu, Jingyu Shi
Methodology: Tong Zhu, Renhao Ni, Haowen Sun, Xu Cao, Shang Chen
Writing–original draft: Tong Zhu, Renhao Ni
Writing–review & editing: Hua Zhang, Yang Luo, Lu Yang

Ethics approval and consent to participate

Not applicable.

Consent for publication

Not applicable.

Availability of data

The datasets generated and/or analyzed during the current study are not publicly available due to ongoing studies, but are available from the corresponding author upon reasonable request.

References

1. Meek KM, Knupp C, Lewis PN, Morgan SR, Hayes S. Structural control of corneal transparency, refractive power and dynamics. *Eye*. 2025;39(4):644-650. doi: 10.1038/s41433-024-02969-7.

2. Brown L, Leck AK, Gichangi M, Burton MJ, Denning DW. The global incidence and diagnosis of fungal keratitis. *Lancet Infect Dis.* 2021:21(3):e49-e57. doi: 10.1016/s1473-3099(20)30448-5.

3. Gain P, Jullienne R, He Z, *et al*. Global survey of corneal transplantation and eye banking. *JAMA Ophthalmol.* 2016:134(2):167-173. doi: 10.1001/jamaophthalmol.2015.4776.

4. Deogaonkar K, Roy A. Donor related corneal graft infection: a review of literature and preventive strategies. *Semin Ophthalmol.* 2023:38(3):219-225. doi: 10.1080/08820538.2022.2095873.

5. Weiss JS, Rapuano CJ, Seitz B, *et al*. IC3D classification of corneal dystrophies-Edition 3. *Cornea.* 2024:43(4): 466-527. doi: 10.1097/ico.0000000000003420.

6. Rafat M, Jabbarvand M, Sharma N, *et al*. Bioengineered corneal tissue for minimally invasive vision restoration in advanced keratoconus in two clinical cohorts. *Nat Biotechnol.* 2023;41(1):70-81. doi: 10.1038/s41587-022-01408-w.

7. Li Y, Wang Z. Biomaterials for corneal regeneration. *Adv Sci.* 2025;12(6):e2408021. doi: 10.1002/advs.202408021.

8. Maher C, Chen Z, Zhou Y, *et al*. Innervation in corneal bioengineering. *Acta Biomater.* 2024;189:73-87. doi: 10.1016/j.actbio.2024.10.009.

9. Camburu G, Zemba M, Tătaru CP, Purcărea VL. The measurement of central corneal thickness. *Rom J Ophthalmol.* 2023;67(2):168-174. doi: 10.22336/rjo.2023.29.

10. Vijayaraghavan R, Loganathan S, Valapa RB. 3D bioprinted photo crosslinkable GelMA/methylcellulose hydrogel mimicking native corneal model with enhanced in vitro cytocompatibility and sustained keratocyte phenotype for stromal regeneration. *Int J Biol Macromol.* 2024;264(Pt 1):130472. doi: 10.1016/j.ijbiomac.2024.130472.

11. Cai Y, Tan Y, Cao J, *et al*. Dual-crosslinked betaine-based amphiphilic hydrogel as a promising vitreous substitute: anti-adhesion, anti-fouling, and anti-cell proliferation. *Adv Sci.* 2025;12(36):e13455. doi: 10.1002/advs.202413455.

12. Kim JJ, Bae M, Kim J, *et al*. Development of a 3D cell-printed RVO model by advancing a retina-on-a-chip with hybrid retinal dECM bioink and an integrated 3D bioprinting system. *Adv Compos Hybrid Mater* 2025; 8(5):364. doi: 10.1007/s42114-025-01455-2.

13. Chand R, Janarthanan G, Elkhoury K, Vijayavenkataraman S. Digital light processing 3D bioprinting of biomimetic corneal stroma equivalent using gelatin methacryloyl and oxidized carboxymethylcellulose interpenetrating network hydrogel. *Biofabrication*. 2025;17(2). doi: 10.1088/1758-5090/adab27.

14. Xu Y, Liu J, Song W, *et al*. Biomimetic convex implant for xorneal regeneration through 3D printing. *Adv Sci.* 2023;10(11):e2205878. doi: 10.1002/advs.202205878.

15. Goodarzi Hosseinabadi H, Dogan E, Miri AK, Ionov L. Digital Light processing bioprinting advances for microtissue models. *ACS Biomater Sci Eng.* 2022;8(4):1381-1395. doi: 10.1021/acsbiomaterials.1c01509.

16. Chen A, Wang W, Mao Z, *et al*. Multimaterial 3D and 4D bioprinting of heterogenous constructs for tissue engineering. *Adv Mater.* 2024;36(34):e2307686. doi: 10.1002/adma.202307686.

17. Grönroos P, Mörö A, Puistola P, *et al*. Bioprinting of human pluripotent stem cell derived corneal endothelial cells with hydrazone crosslinked hyaluronic acid bioink. *Stem Cell Res Ther.* 2024;15(1):81. doi: 10.1186/s13287-024-03672-w.

18. Ouyang L, Yao R, Mao S, *et al*. Three-dimensional bioprinting of embryonic stem cells directs highly uniform embryoid body formation. *Biofabrication*. 2015; 7(4):044101. doi: 10.1088/1758-5090/7/4/044101.

19. Shi B, Zhu T, Luo Y, *et al*. Three-dimensional bioprinted cell-adaptive hydrogel with anisotropic micropores for enhancing skin wound healing. *Int J Biol Macromol.* 2024;280(Pt 4):136106. doi: 10.1016/j.ijbiomac.2024.136106.

20. Guo K, Li G, Yu Q, *et al*. Injectable hyaluronate-based hydrogel with a dynamic/covalent dual-crosslinked architecture for bone tissue engineering: enhancing osteogenesis and immune regulation. *Int J Biol Macromol.* 2024;282(Pt 5):137249. doi: 10.1016/j.ijbiomac.2024.137249.

21. Asim S, Tuftee C, Qureshi AT, *et al*. Multi-functional gelatin-dithiolane hydrogels for tissue engineering. *Adv Funct Mater.* 2025;35(3):2407522. doi: 10.1002/adfm.202407522.

22. Puistola P, Miettinen S, Skottman H, Mörö A. Novel strategy for multi-material 3D bioprinting of human stem cell based corneal stroma with heterogenous design. *Mater Today Bio.* 2024;24:100924. doi: 10.1016/j.mtbio.2023.100924.

23. Ahn M, Park GT, Shukla AK, *et al*. 3D Bioprinting-assisted engineering of stem cell-laden hybrid biopatches with distinct geometric patterns considering the mechanical characteristics of regular and irregular connective tissues. *Adv Healthc Mater.* 2025;14(25):e2502763. doi: 10.1002/adhm.202502763.

24. Xu R, Zhang H, Luo Y, *et al*. Magnetically bioprinted anisotropic hydrogels promote BMSC osteogenic differentiation for bone defect repair. *Mater. Today Bio.* 2025;32:101885.
doi: 10.1016/j.mtbio.2025.101885.

25. Sang S, Yan Y, Shen Z, *et al*. Photo-crosslinked hydrogels for tissue engineering of corneal epithelium. *Exp Eye Res.* 2022;218:109027.
doi: 10.1016/j.exer.2022.109027.

26. Zhang H, Luo Y, Hu Z, *et al*. Cation-crosslinkedκ-carrageenan sub-microgel medium for high-quality embedded bioprinting. *Biofabrication*. 2024;16(2).
doi: 10.1088/1758-5090/ad1cf3.

27. Zhang H, Luo Y, Li G, *et al*. Micelle-facilitated gelation kinetics and viscoelasticity of dynamic hyaluronan hydrogels for bioprinting of mimetic constructs and tissue repair. *Composites, Part B: Eng.* 2025;294:112151.
doi: 10.1016/j.compositesb.2025.112151.

28. Larrañeta E, Henry M, Irwin NJ, *et al*. Synthesis and characterization of hyaluronic acid hydrogels crosslinked using a solvent-free process for potential biomedical applications. *Carbohydr Polym.* 2018;181:1194-1205.
doi: 10.1016/j.carbpol.2017.12.015.

29. Velasco-Rodriguez B, Diaz-Vidal T, Rosales-Rivera LC, *et al*. Hybrid methacrylated gelatin and hyaluronic acid hydrogel scaffolds. preparation and systematic characterization for prospective tissue engineering applications. *Int J Mol Sci.* 2021;22(13).
doi: 10.3390/ijms22136758.

30. Zhou M, Yue K, Zhao J, *et al*. Optimizing GBM organoid construction with hydrogel-based models: GelMA-HAMA scaffold supports GBM organoids with clonal growth for drug screening. *Cell Transplant.* 2025;34:9636897251347537.
doi: 10.1177/09636897251347537.